Pergamon

Journal of Structural Geology, Vol. 17, No. 2, pp. 257 to 264, 1995
Elsevier Science Ltd
Printed in Great Britain
0191-8141/95 $9.50+0.00

0191-8141(94)00051-4

The effects of rupture and diffusion on the salinity of fault-related fluid inclusions

KIERAN D. O'HARA

Department of Geological Sciences, University of Kentucky, Lexington, KY 40506, U.S.A.

(*Received* 30 *October* 1992; *accepted in revised form* 25 *March* 1994)

Abstract—The combined effects of fault rupture and diffusive transport on the salinity of fault-related fluids are addressed in the case of both an external solute source and that of rock buffered fluid compositions. The effects of injection of a dilute and a saline fluid into a fault zone, followed by diffusion, are examined in the case of both periodic and random fault rupture events. The models reproduce the large salinity variations characteristic of fault-related secondary fluid inclusions, and suggest that correlation of salinity variations may allow reconstruction of rupture events.

In the case of rock buffered fluid compositions, the hydration of periclase to form brucite is used as a simple petrological model for increasing salinity in fault zones. An episodic hydration reaction, both with and without dilution effects, is capable of increasing the salinity of small volumes of fluid along microfractures and also of producing large salinity variations.

These considerations suggest that large salinity variations and high fluid concentrations common in secondary fluid inclusions associated with retrograde shear zones may be due to the combined effects of diffusion and rock buffering reactions in the fault zone. The concentration spikes produced during rupture are damped by diffusion with increasing distance from the site of rupture. Concentration peaks and troughs coincide in time at different distances from the source suggesting the possibility of correlating salinity variations in the vicinity of a fault zone.

INTRODUCTION

The importance of fluid-rock interaction coupled with tectonic activity is widely recognized, particularly in the fields of ore genesis (e.g. Sibson 1987), earthquake studies (e.g. Scholz *et al.* 1973), and the behavior of faults and shear zones in general (e.g. Sibson *et al.* 1975, Kerrich 1989, Byerlee 1993). Active faults are the locus of fluid compositional and thermal anomalies (Vrolijk *et al.* 1991) and sharp fluctuations in ground water composition are often associated with seismic events (Thomas 1988). The compositional evolution of tectonically-derived fluids is likely to be complex, involving the coupling of mechanical, chemical, thermal and hydrological processes (Tsang 1991).

Fluid inclusion studies of fault-related rocks offer a unique opportunity to gain information on the compositional evolution of such fluids. Microstructures indicate that inclusions are commonly trapped at the time of tectonic activity, for example, crack-seal texture (Ramsay 1980). Despite deformation-related effects such as inclusion stretching and volume changes, inclusions commonly maintain their original salinity (e.g. Sterner & Bodnar 1989). Also, most secondary fluid inclusions in deformed rocks are trapped along healed microfractures in quartz, and experimental studies indicate that such microcracks heal rapidly (e.g. years; Smith & Evans 1984). The time required for crack healing depends on fluid salinity, temperature and crack length. For example, at temperatures of 300°C, cracks 100 μ in length will heal in aqueous fluid in less than a year (Brantley *et al.* 1990). A given population of microcracks, however, is likely to have a wide range of healing times.

Planes of secondary fluid inclusions are often related to distinct tectonic events. Transgranular fluid inclusion trails commonly have a strong preferred orientation and are thought to form in the plane of the intermediate and maximum principal stress (Engelder 1987). In experimental rock deformation studies, microcrack arrays form as tensile fractures during pre-rupture events (Costin 1987) and correspondence between acoustic emissions and microcrack arrays suggests that the arrays formed in response to specific deformation events (Scholz 1990). In studies of natural rocks it is also commonly inferred that trails of secondary inclusions are related to specific tectonic events (Kowalis *et al.* 1987, Lespinasse & Cathelineau 1990, O'Hara 1991). In the presence of a fluid, the displacement of the crack walls can be expected to draw fluid into the crack, leading to crack healing (Shelton & Orville 1980, Smith & Evans 1984) and resulting in the formation of fluid inclusions (Roedder 1984). These considerations suggest that secondary fluid inclusions trapped along healed microfractures can be expected to preserve a record of fluid composition during tectonic events on geologically short time scales.

Secondary fluid inclusion salinities

A characteristic feature of fluid inclusion compositions in faults and shear zones is their highly variable salinity (e.g. Crawford 1981, Guha *et al.* 1983, Bennett & Barker 1992, O'Hara & Haak 1992). In a study of fluid

inclusions on the Rector Branch thrust, North Carolina, the latter workers showed that salinities ranged from 3 to 25 wt% NaCl equivalent, with variations of greater than 15 wt% within individual quartz vein samples on the thin section scale. First melting temperatures (−25.5 to −32.5°C) indicate solutes such as $CaCl_2$ were present in addition to NaCl, and minimum salinities tend to decrease toward the fault zone. Secondary fluid inclusions from the nearby Meadow Fork fault zone also show a wide range but the majority have a salinity of 18–25 wt% NaCl equivalent (O'Hara 1990). Secondary fluid inclusions associated with two different alteration assemblages on the Wasatch normal fault, Utah, (Parry *et al.* 1988) show salinities of 5–17 wt% and of 2–16 wt % NaCl equivalent, respectively. Thrust zones associated with Caledonian retrograde metamorphism in northern Norway contain fluid inclusions with salinities in the range of 27–50 wt% (Bennett & Barker 1992). Where effects such as boiling and immiscibility can be ruled out, these salinities require major changes in fluid composition with time. Processes such as membrane filtration (Hanor 1979) and radiolytic enrichment (Vovk 1987) can also be ruled out as these processes tend to increase salinity uniformly in space and also over protracted periods of time.

Variable salinities are to be expected in tectonically active areas where repeated pulsing of fluid is likely to result in rapid compositional changes. The most common explanation for these salinity variations is mixing of fluid reservoirs of different provenance. This could be an important process where fluid reservoirs are tectonically juxtaposed. In cases where the source of formation waters or other saline fluids is not apparent (for example, in crystalline terranes), the alternative possibility is that chemical reaction in the rock buffered the fluid composition. In the Canadian shield, for example, ground water at a depth greater than about 1 km commonly contains 30 wt% total dissolved solids. The composition of these fluids is consistent with low temperature (25–100°C) fluid–rock interaction in which the fluid composition is buffered by chemical reaction (e.g. Frape & Fritz 1986, Gascoyne *et al.* 1986). Fluid inclusion studies also indicate that fluid composition can reflect the host rock composition (Crawford *et al.* 1979, Bennett & Barker 1990). The latter workers have shown that the composition of fluid inclusions was internally buffered by the equilibrium between mica and feldspar in the host rocks. In southeast Pennsylvania, $CaCl_2$–NaCl brines occur in calcium-rich retrograde lithologies, whereas NaCl brines are associated with calcium-poor lithologies, also suggesting buffering of fluid composition by the host lithology (Crawford *et al.* 1979).

The role of chemical reactions in buffering fluid composition is well known to metamorphic petrologists (Greenwood 1975) and hydrolysis and hydration reactions have been implicated in altering salinity of fluid inclusions (e.g. Crawford *et al.* 1979). Hydration reactions can increase the concentration of dilute fluid by removing H_2O and incorporating it into the hydrous phase. This mechanism has the advantage that an additional source of anions (e.g. Cl^-) is not required to increase salinity. Evaporite sequences or seawater are commonly cited as a source for these ions in saline fluids (Cole 1983, Roedder 1984).

The first part of this paper addresses the role of an external source of salinity in fault zones and the role of diffusive transport in a porous fault zone matrix in determining fluid inclusion salinity. The second part examines the role of hydration reactions in buffering the composition of small volumes of fluid trapped along microfractures in an active fault zone. The objective is to gain insight into the possible tectonic significance of the salinity variations observed in fault-related fluid inclusions.

EXTERNAL SOLUTE SOURCE AND DIFFUSIVE TRANSPORT

The model

The transport properties of the fault zone being considered are based on the analysis of Norton & Knapp (1977) in which porosity comprises a flow porosity, representing conduits for fluid flow, and a diffusive porosity, in which transport is by solute diffusion in the fluid. Diffusion pores are either discontinuous or have too small an aperture to allow fluid flow. It is along the latter that secondary fluid inclusions are usually trapped (e.g. Roedder 1984), particularly in faults and shear zones (Parry *et al.* 1988, Lespinasse & Cathelineau 1990, O'Hara 1991). It is assumed that these pores initially become filled with fluid during dilatancy events associated with fault rupture. Studies of fluid inclusions produced experimentally along healed microfractures in quartz indicate that transport is by diffusion in the fluid rather than advection of the fluid (Smith & Evans 1984). The flow porosity is inferred to consist of fractures and the spacing between these fractures will determine the distance over which diffusive transport takes place (Norton & Knapp 1977).

In the models considered, diffusion of solute into a fault zone matrix occurs until fault rupture results in one of two types of behavior: either the fault matrix is flushed with dilute externally derived fluid, thereby resetting the salinity to zero, or injection of a 'spike' of solute occurs resulting in increased salinity. The frequency of faulting is therefore an important variable in both types of model.

Fault recurrence intervals

Fault recurrence intervals for large earthquakes are variable and may depend on tectonic setting. A recurrence interval of 3000 years is estimated for the normal faulting in the Aegean region (Armijo *et al.* 1991). Recurrence intervals of surface ruptures on the Wasatch normal fault, during the past 8000 y, are estimated to be 400–666 y (Schwartz & Coppersmith 1984) with esti-

mates for individual segments of up to 3000 y. For large events on the northern San Andreas fault, typical intervals are 200–300 y (Niemi & Hall 1992). Because the frequency–magnitude relationship for earthquakes obeys a power-law relationship, smaller events can be expected to be much more frequent (e.g. Scholz 1990, p. 187). For example, moderate sized events on the San Andreas at Parkfield have a recurrence interval of 21 y (Scholz 1990). Time scales on the order of 10^2–10^3 years appear to be appropriate when considering the frequency of large to moderate-sized rupture events.

Periodic rupture

In this model, a large volume of externally derived dilute fluid periodically flushes the fault zone and reduces the salinity to zero. The solute concentration then increases again by diffusion of solute into the fault zone during periods of fault stability. The combined effects of diffusion and periodic rupture are examined.

A solution to the diffusion equation:

$$\partial C/\partial t = D\ \partial^2 C/\partial x^2 \qquad (1)$$

for a plane source deposited at the surface of a semi-infinite medium is (equation 3.13 in Crank 1976):

$$C = C_e + (C_0 - C_e)\ \mathrm{erf}\ (x/\sqrt{[4Dt]}) \qquad (2)$$

where D is the diffusion coefficient ($m^2\ s^{-1}$), x is distance (m), t is time (s) and C_e is the equilibrium concentration. C_0 is the initial concentration throughout the fault zone, so that the initial condition is:

$$C(x, t) = C_0,\ x > 0,\ t = 0.$$

Because the source represents a large reservoir the equilibrium concentration C_e at the surface of the porous medium (i.e. the fault zone) between rupture events is constant so that:

$$C(x, t) = C_e,\ x = 0,\ t \geq 0$$

represents a boundary condition. Parenthetically, it is pointed out that with the initial condition $C_0 = 0, x > 0$, $t = 0$, the better known solution to equation (1) is $C = C_0\ \mathrm{erfc}\ (x/\sqrt{[4Dt]})$. In some of the models presented below, however, the salinity increases are additive during repeated tectonic events, so that $C_0 \neq 0$ at the beginning of each tectonic cycle, except in the case of the first event.

The diffusion coefficient for NaCl in water at 25°C is $1.5 \times 10^{-9}\ m^2\ s^{-1}$ and is only weakly dependent on temperature and pressure. Between 200 and 500°C at 2 kbar, for example, the tracer diffusion coefficient for NaCl ranges from 10^{-8} to $4 \times 10^{-8}\ m^2\ s^{-1}$ (Oelkers & Helgeson 1988). A value of $10^{-8}\ m^2\ s^{-1}$ is used in this study. This value must be multiplied by a geometric factor to take into account the retardation effects of the rock matrix, to give an effective diffusion coefficient D_e (Neretnieks 1980). The geometric factor is strongly dependent on confining pressure and porosity. Over a wide range of porosities, the geometric factor equals the porosity. For example, with a porosity of 1%, a geometric factor on the order of 10^{-2} is appropriate for diffusion in granitic rock (Neretnieks 1980). At deeper levels both temperature and pressure will tend to reduce porosity due to crack healing and pore closure (e.g. Brenan 1991). Extrapolation of data for various granitic rocks from a porosity of 0.005 (at 50 Mpa) to a porosity of 0.001 gives a geometric factor of 10^{-4} (Neretnieks 1980). Thus geometric factors of 10^{-2}–10^{-4} should be representative of deeper level brittle faults and brittle–plastic shear zones. This would correspond to effective diffusion coefficients, D_e, of 10^{-10}–$10^{-12}\ m^2\ s^{-1}$. These values will provide minimum diffusion distances if applied to shallower level structures where diffusivity is expected to be faster.

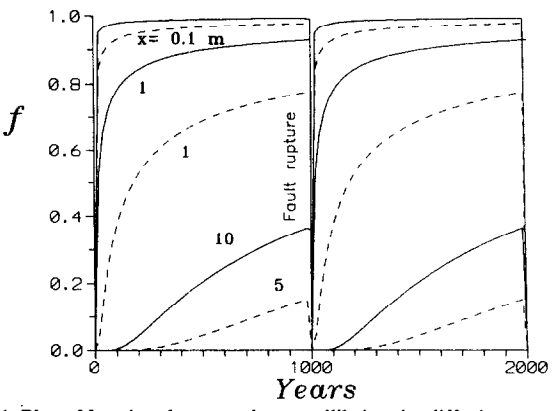

Fig. 1. Plot of fractional approach to equilibrium by diffusive transport at various distances (in meters) into a semi-infinite medium from a plane source for a fault recurrence interval, r, of 10^3 y. $D_e = 10^{-12}\ m^2\ s^{-1}$ (dashed curves) and $10^{-11}\ m^2\ s^{-1}$ (solid curves). The concentration curves were obtained by iteration of equation (2). The fluid concentration is reset to zero after each rupture event.

The concentration as a function of distance and time can be evaluated using equation (2) above. The maximum concentration after the first rupture event occurs when $t = r$, where r is the fault recurrence interval:

$$C_{max} = C_e + (C_0 - C_e)\ \mathrm{erf}\ (x/\sqrt{[4Dr]}). \qquad (3)$$

The minimum concentration, $C_{min} = C_0$ when $t = 0$.

Figure 1 shows the fractional approach to equilibrium, $f(=C/C_e)$, for various distances, using a fault recurrence interval r of 10^3 y and D_e values of $10^{-11}\ m^2\ s^{-1}$ (solid lines) and $10^{-12}\ m^2\ s^{-1}$ (dashed lines). For short distances (0.1–1 m) the approach to equilibrium is rapid (<100 y) resulting in a step like concentration profile with time, whereas for greater distances (5–10 m) a more gradual increase in concentration occurs. It can be seen from Fig. 1 that for more active faults, (i.e. shorter recurrence intervals) a lower fluid concentration would be obtained at a given distance from the source, and conversely, a higher concentration would be obtained for less active faults.

Random rupture events

A shortcoming of the model above is that the value of C_e is kept constant for each tectonic event, and also that the tectonic events are strictly periodic. It might be suggested, on the basis of the seismic pumping hypoth-

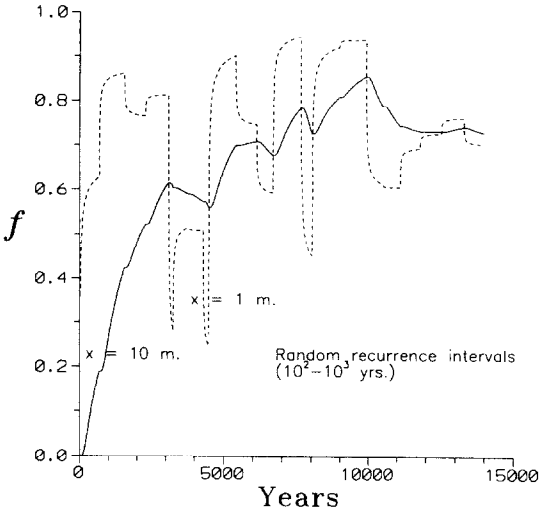

Fig. 2. Concentration profiles due to diffusion for random recurrence intervals between 10^2 and 10^3 y. C_e is proportional to the recurrence interval. The initial concentration, C_0, equals C_{max} from the previous event. Note that although variations in concentration are damped at greater distances from the source, the troughs and peaks in both curves coincide. $D_e = 10^{-11}$ m^2 s^{-1}. $x = 1$ m (dashed curve) and $x = 10$ m (solid curve).

esis (Scholz *et al.* 1973, Sibson 1987), that larger tectonic events would introduce larger volumes of fluid, thereby producing greater salinity changes whereas smaller events would cause less change. In addition, fault recurrence intervals are averages, sometimes averaged over several faults or fault segments (Schwartz & Coppersmith 1984). Actual fault activity is likely to be much more variable. These factors can be taken into account by assigning 'random' recurrence intervals in which the increase in the value of C_e is proportional to the recurrence interval. For example, if C_e is assigned a value of 0.1 for a random recurrence interval of 100 y, C_e would equal 0.2 for an interval of 200 y. In contrast to the model above, values of C_e may be less than C_0, in which case the direction of diffusion is reversed (i.e. diffusion out of the fault zone). As before, C_e is constant between faulting intervals.

Figure 2 shows the evolution of the system at a distance of 1 m (dashed line) and 10 m (solid line) from the source, for random recurrence intervals of 10^2–10^3 y. The curves were produced by iterating equation (2) using a BASIC routine (Appendix). Both curves in Fig. 2 are responding to the same sequence of random events. It can be seen that highly variable concentrations occur 1 m from the fault, whereas at 10 m these variations are considerably damped by diffusion. This model underscores the conclusion that secondary fluid inclusions trapped close to the site of rupture are likely to show large salinity variations, whereas inclusions trapped farther away show much less variation. An additional notable feature is that increases and decreases in concentration coincide in both curves (Fig. 2) suggesting the possibility, in principle at least, of correlating tectonic events in a fault zone on the basis of fluid inclusion salinity variations.

HYDRATION REACTIONS

Hydration reactions involve the formation of hydrous minerals by consumption of pure H_2O, resulting in an increase in the salinity of the residual fluid. Common reactions in faults and shear zones include the retrogression of amphibole to biotite or chlorite, of plagioclase feldspar to clinozoisite, and of olivine to serpentine (e.g. Beach 1980). For example:

$$Na^+ + 2CaAl_2Si_2O_8 + 2\,SiO_2 + H_2O$$
$$\text{Plagioclase}$$
$$= NaAlSi_3O_8 + CaAl_3Si_3O_{12}(OH) + H^+$$
$$\text{Albite} \qquad \text{Clinozosite}$$

or

$$2KAlSi_3O_8 + 5Mg^{+2} + 8H_2O$$
$$\text{K-feldspar}$$
$$= Mg_5Al_2Si_3O_{10}(OH)_8 + 2K^+ + 8H^+ + 3SiO_2.$$
$$\text{Chlorite}$$

In each of these reactions the extent of reaction will control the increase in salinity of the co-existing fluid. For the purpose of examining possible salinity variations, the hydration of periclase to form brucite in the presence of a brine is used as a model for these more complex reactions:

$$MgO + H_2O\text{–}NaCl = Mg(OH)_2 + H_2O\text{–}NaCl \quad (4)$$

periclase + brine = brucite + more saline brine.

Although the minerals involved in reaction (4) are unlikely to be important in real fault zones, this reaction is used as a simple petrological model for more complex reactions because the composition of brine in equilibrium with the solid phases for this reaction is well characterized (Franz 1982) and also because NaCl is commonly the major component in fault-related fluid inclusions.

With three components (MgO, H_2O and NaCl) and three phases, the phase rule indicates this reaction has two degrees-of-freedom. At fixed P and T therefore, the salinity of the fluid co-existing with the two solid phases is fixed. A schematic phase diagram for this system (Franz 1982) is shown in Fig. 3, where at constant pressure, the reaction is univariant. If we choose a particular temperature, then the salinity of the fluid is specified. If cooling occurs at constant pressure, brucite is stabilized over periclase and for equilibrium to be restored, the salinity of the fluid must increase (at constant temperature) because H_2O is removed from the fluid to form brucite. Assuming local equilibrium is rapidly obtained, this increase in salinity will be essentially instantaneous. Because of the small volume of fluid along microfractures, hydration reactions in the rock will have the ability to buffer the fluid composition. If these microfractures heal rapidly the resulting secondary fluid inclusions will record this salinity increase. On the other hand, longer or wider microfractures can be expected to remain unhealed for longer periods (Brenan

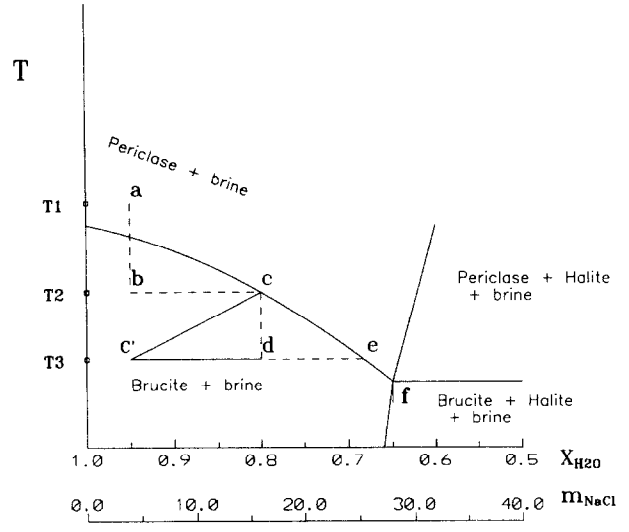

Fig. 3. Schematic phase diagram for the hydration reaction MgO + H_2O–NaCl = $Mg(OH)_2$ + H_2O–NaCl (after Franz 1982). The fluid compositional evolution for episodic dilution and cooling is shown by the curve a–b–c–c′–e. The effect of diffusion on concentration for this situation is modeled in Fig. 4(a). The increase in salinity of the fluid due to episodic cooling without dilution is shown by the dashed curve a–b–c–d–e. The effect of diffusion on concentration for this situation is modeled in Fig. 4(b).

1991) and will be open to subsequent changes in fluid composition by diffusion. Experimental studies and studies of natural rocks indicate that transport along microfractures is by diffusion, rather than advection (Smith & Evans 1984, Fisher & Brantley 1992). Because the healing time of all such microfractures is short compared to the fault recurrence intervals (see Introduction) the resulting fluid inclusion population should provide a record of the changing fluid salinity with time.

As an example, consider a mole of fluid with composition X_{NaCl} = 0.05 co-existing with periclase at temperature T_1 (point a, Fig. 3). This fluid would contain 2.9 g NaCl (and 17.1 g H_2O). This fluid may represent a connate pore fluid. Injection of a lower temperature dilute fluid during fault rupture is inferred to cause cooling of the system to T_2 where brucite is stable (point b, Fig. 3). Equilibrium will be re-established, at constant temperature (c, Fig. 3) by hydration of periclase to form brucite and the salinity of small volumes of fluid along microfractures will increase. If a second rupture event introduces a fluid of the same initial composition at a lower temperature (T_3) the fluid will be diluted along the solid line c–c′(Fig. 3). Additional chemical reaction will tend to restore equilibrium at constant temperature (along c′–d–e, Fig. 3) and the cycle is repeated. If periodic fault rupture causes cooling *without* dilution then the path of the fluid composition will follow the dashed curve a–b–c–d–e–f (Fig. 3). Under these circumstances the salinity increases are cumulative. At the invariant point (f, Fig. 3) the fluid becomes saturated with halite, and no further cooling can occur until either all the periclase or solution is used up. At this point the fluid composition is X_{NaCl} = 0.35. Because NaCl has not been added or removed from the system the fluid still contains 2.9 g NaCl. However, because X_{H_2O} = 0.65, only 1.7 g of H_2O are present. This requires removal of 15.4 g or 0.85 moles of water during hydration to produce this fluid composition. Since brucite is formed from equal molar quantities of H_2O and periclase, it follows that 0.85 moles or 34.6 g of periclase are required to buffer one mole (20 g) of starting fluid to the point of saturation. These considerations indicate that chemical hydration has the ability to buffer the concentration of a substantial volume of low salinity fluid.

Cooling and diffusion

The two paths described above (Fig. 3) represent two end-member models in which (1) episodic cooling but no dilution of the fault zone fluid occurs and (2) the case in which both cooling and dilution of the fluid occur during rupture. Diffusion is likely to modify the salinity of fluid as a function of distance from the site of chemical reaction and this effect, together with periodic fault rupture events, is examined below.

In these models the value of C_e increases incrementally after each rupture event but remains constant between events. The incremental increase in C_e will depend on the slope of the equilibrium curve in T–X space for the specific reaction of interest and also on the amount of cooling. In the case of reaction (4) the increase in fluid concentration to saturation occurs over an 80°C interval (Franz 1982). In the real crust the retrogression of amphibolite to greenschist, for example, involves the addition of only about 5 wt% H_2O, which would result in lower salinities. A somewhat arbitrarily value of C_e = 0.1 m for each cooling event is used in the models below.

Episodic cooling with dilution

Because total dilution of the fault zone fluid occurs by the incoming fluid the initial condition after each tectonic event is $C_0(x,t) = 0$, $t = 0$. The effect of diffusive transport as a function of distance for a fault recurrence interval of 10^3 y for different diffusion coefficients was evaluated by iterating equation (2) above (Fig. 4a). Equilibrium is rapidly attained close to the source (x = 0.1–1 m) when $D_e = 10^{-10}$ m^2 s^{-1} giving rise to a staircase profile, whereas for a lower value of D_e (10^{-12} m^2 s^{-1}) at the same distance, the approach to equilibrium is more gradual. At a distance of 10 m and the same D_e value, only a fractional approach to equilibrium is attained. Although the concentration maxima become smaller with distance from the source, the breaks in slopes of the curves at various distances are synchronous, suggesting that salinity peaks in samples at different distances from the source may reflect the same rupture event.

Episodic cooling without dilution

As before, C_e increases incrementally at each rupture event and is held constant between rupture events. But, because no dilution occurs during fault rupture the salinities are additive. In this case, the initial salinity, C_0,

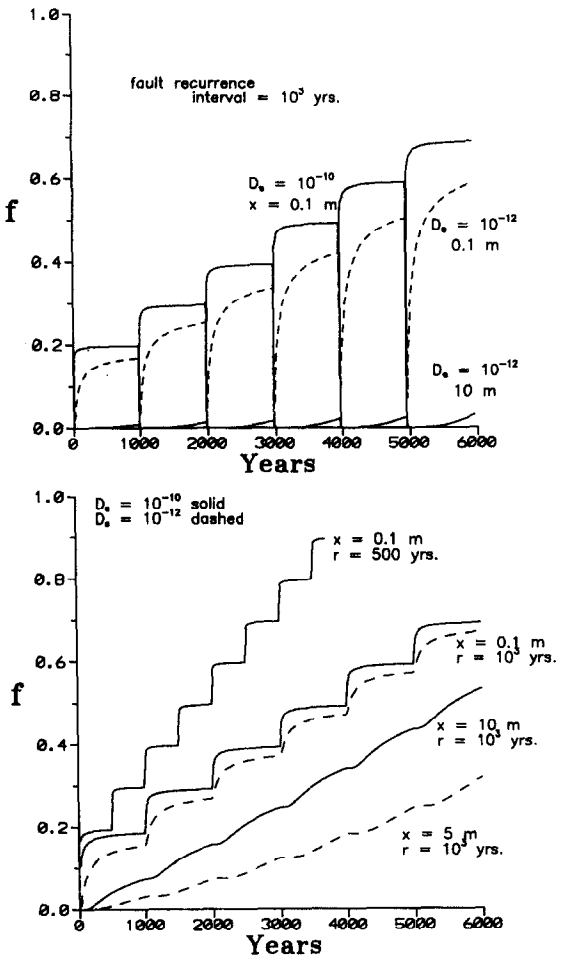

Fig. 4. (a) Plot of concentration versus time due to diffusion for a recurrence interval of 10^3 y for different values of x and D_e. The equilibrium concentration $(C)_e$ is episodically increased by 0.1 m and the salinity is reset to zero after each rupture event. See path a–b–c–c′–d–e in Fig. 3. (b) Plot of fluid concentration versus time for periodic cooling in a fault, without dilution, (see path a–b–c–d–e, Fig. 3). Fluid concentration is additive and C_e increases incrementally by 0.1 m after each rupture event. The concentration near the source displays a stepped shape and the steps are attenuated at greater distances from the source and also for lower values of D_e. Shorter recurrence intervals (e.g. r = 500 y) result in higher salinities. D_e values are indicated.

at the beginning of each tectonic cycle will be equal to the maximum salinity, C_{max}, at the end of the previous cycle, so that:

$$C_{max}^{n-1} = C_0^n$$

where C_0^n is the initial concentration for the nth rupture event. The maximum salinity obtained at the end of the second cycle, C_{max}^2, for example, is given by substituting C_{max} in equation (3) for C_0 in equation (2) and letting $t = r$:

$$C_{max}^2 = C_e' + \{[C_e + (C_0 - C_e)\ \mathrm{erf}\ (y)] - C_e'\}\ \mathrm{erf}\ (y) \quad (5)$$

where C_e' is the new equilibrium concentration and $y = x/\sqrt{4Dr}$). For large values of r (i.e. long fault recurrence intervals), y tends to zero and equation (5) reduces to $C_{max}^2 = C_e'$ [note: erf(0) = 0]. Thus, the maximum possible concentration is simply the new equilibrium concentration. Figure 4(b) shows the evolution of the system at different times and distances for a recurrence interval of 10^3 y for $D_e = 10^{-12}$ m^2 s^{-1} (dashed curves) and 10^{-11} m^2 s^{-1} (solid curves). Close to the source (0–1 m) the salinity evolution has a staircase profile reflecting the rapid increase in salinity near the source. Farther from the source, diffusion attenuates these steps resulting in a more gradual increase in salinity. Because salinity spikes are additive, however, higher concentrations are possible (compare Fig. 4a). Shorter recurrence intervals result in more rapid salinity increases, and longer intervals result in slower increases. On the basis of this model, arbitrarily high salinities can be obtained (up to fluid saturation), given a sufficiently large number of rupture events and sufficiently large incremental increases in C_e. Diffusion is seen to be effective in damping salinity fluctuations at distances greater than a few meters from the source. This result suggests that the magnitude of the compositional fluctuations reflect proximity to a tectonically active source.

DISCUSSION

Although the models outlined above cannot distinguish between a rock buffered fluid and an external fluid source, they do demonstrate that, depending on the fault recurrence interval, fault rupture is capable of inducing abrupt salinity variations in a fault zone fluid. It is argued that samples of these variable salinity fluids will be trapped as secondary fluid inclusions. In the case of a fault zone into which solute is continuously diffusing from an external source and also periodically flushed by a dilute fluid, it was shown that active faults with short recurrence intervals result in lower fluid salinities, and less active faults with longer recurrence intervals produce higher salinities.

In the case of rock-buffered fluid compositions, it is suggested that, using the hydration of periclase to form brucite as a model, that hydration reactions can increase fluid salinity by consuming H_2O during episodic cooling events. The hydration of periclase to form brucite is not intended to represent a typical example of hydration reaction in a fault zone, but rather it is used solely to model the likely effects of hydration on fluid composition. The cooling events in the model correspond to injection of cold fluid during fault rupture. In this case, more active faults produce higher salinities. If an externally derived low salinity fluid (e.g. seawater) is present as a pore fluid, then hydration reactions can increase concentration, depending on the extent of reaction. In this regard, hydration reactions are important because they can increase salinity by concentrating already existing solute during cooling so that an external source of solute is not required. It appears possible that similar reactions produced the high salinity fluids observed in sheared rocks of the Henderson mine (Guha *et al.* 1983) and also along thrusts in the Caledonides of Norway (Bennett & Barker 1992) and the Blue Ridge province of the southern Appalachians (e.g. O'Hara & Haak 1992). The models also successfully reproduce the large salinity fluctuations commonly observed along such fault zones.

Because the peaks and troughs on salinity curves coincide in time (e.g. Figs. 2 and 4a) the suggestion was made that tectonic events might be correlated in the vicinity of a fault zone on the basis of salinity variations in samples at different distances from the site of rupture. The correlation of fluid inclusion populations on the basis of morphological, textural, compositional and other characteristics has been described by many workers (e.g. Roedder 1984, p. 429–435). It is commonly possible to establish a chronological sequence of fluid inclusion populations on the basis of growth zones in crystals, for example, allowing fluid composition to be plotted against time. Although establishing a chronology of fluid inclusion generations in fault zones is usually difficult, sharp variations in fluid inclusion salinities might be correlated in different samples, thereby allowing the reconstruction of rupture events. The models indicate compositional fluctuations are damped by diffusive processes at distances greater than a few meters (e.g. Fig. 2), suggesting that the magnitude of salinity variations reflect the distance from the rupture site. Because of the approximate relationship $x \approx \sqrt{(Dt)}$, the distance over which such effects will be visible will depend on the square root of the diffusion coefficient.

Continuous variations in salinity (and also homogenization temperatures) are commonly observed in fluid inclusion studies. These variations are normally attributed to mixing of fluids of different salinity and temperature. As shown here such compositional trends could also be produced by diffusive transport of solute in a fault zone fluid.

Acknowledgements—Some of the ideas presented here were developed while on sabbatical leave at University College Dublin; I thank the faculty and staff there for their hospitality during my stay. Comments on an early draft by Chris Bean and David Johnson were helpful. Journal reviews by William Parry, Steven Wojtal and an anonymous reviewer are gratefully acknowledged. The editorial handling of Steven Wojtal is also appreciated.

REFERENCES

Armijo, R., Lyon-Caen, H. & Papanastassiou, D. 1991. A possible normal-fault rupture for the 464 BC Sparta earthquake. *Nature* **251**, 137–139.

Beach, A. 1980. Retrogressive metamorphism in shear zones with special reference to the Lewisian complex. *J. Struct. Geol.* **2**, 257–263.

Bennett, D. G. & Barker, A. J. 1992. High salinity fluids: the result of retrograde metamorphism in thrust zones. *Geochim cosmochim. Acta* **56**, 81–95.

Brantley, S. L., Evans, B., Hickman, S. H. & Crerar, D. A. 1990. Healing of microcracks in quartz: implications for fluid flow. *Geology* **18**, 136–139.

Brenan, J. M. 1991. Development and maintenance of metamorphic permeability: implications for fluid transport. In: *Contact Metamorphism* (edited by Kerrick, D. M.). *Min. Soc. Am.* Reviews of mineralogy **26**, 291–315.

Byerlee, J. 1993. Model for episodic flow of high-pressure water in fault zones before earthquakes. *Geology* **21**, 303–306.

Cole, D. R. 1983. Chemical and isotopic investigation of warm springs associated with normal faults in Utah. *J. Volcanol. & Geotherm. Res.* **16**, 65–98.

Costin, L. S. 1987. Time-dependent deformation and failure. In: *Fracture Mechanics of Rock* (edited by Atkinson, B. K.). Academic Press, London, 167–215.

Crank, J. 1976. *Mathematics of Diffusion*. Oxford University Press, York.

Crawford, M. L. 1981. Fluid inclusions in metamorphic rocks—low and medium grade. In: *Fluid Inclusions: Applications to Petrology* (edited by Hollister, L. S. & Crawford, M. L.). *Min. Soc. Can.* **6**, 157–176.

Crawford, M. L., Filer, J. & Wood, C. 1979. Saline fluid inclusions associated with retrograde metamorphism. *Bull. Mineral.* **102**, 562–568.

Engelder, T. 1987. Joints and shear fractures in rock. In: *Fracture Mechanics of Rock* (edited by Atkinson, B. K.). Academic Press, London, 27–65.

Fisher, D. M. & Brantley, S. L. 1992. Models of quartz overgrowth and vein formation: deformation and episodic fluid flow in an ancient subduction zone. *J. geophys. Res.* **97**, 20,043–20,061.

Franz, G. 1982. The brucite–periclase equilibrium at reduced H_2O activities: some information about the system H_2O–NaCl. *Am. J. Sci.* **282**, 1325–1339.

Frape, S. K. & Fritz, P. 1986. Geochemical trends from groundwaters from the Canadian shield. In: *Saline Water and Gases in Crystalline Rocks* (edited by Fritz, P. & Frape, S. K.). *Spec. Pap. geol. Ass. Can.* **33**, 19–38.

Gascoyne, M., Davison, Ross, J. D. & Pearson, R. 1986. Saline groundwater and brines in plutons in the Canadian shield. In: *Saline Water and Gases in Crystalline Rocks* (edited by Fritz, P. and Frape, S. K.). *Spec. Pap. geol. Ass. Can.* **33**, 53–68.

Greenwood, H. J. 1975. Buffering of pore fluids by metamorphic reactions. *Am. J. Sci.* **275**, 573–593.

Guha, J., Archamault, G. & Leroy, J. 1983. A correlation between the evolution of mineralizing fluids and the geomechanical development of a shear zone as illustrated by the Henderson 2 mine, Quebec. *Econ. Geol.* **78**, 1605–1618.

Hanor, J. S. 1979. The sedimentary genesis of hydrothermal fluids. In: *Geochemistry of Hydrothermal Ore Deposits* (edited by Barnes, H. L.). Wiley, New York, 137–168.

Kerrich, R. 1989. Geodynamic setting and hydraulic regimes: shear zone hosted mesothermal gold deposits. In: *Mineralization and Shear Zones* (edited by Bursnall, J.). *Geol. Assoc. Can. short course* **6**, 89–128.

Kowalis, B. J., Wang, H. F. & Jang, B. 1987. Healed microcrack orientation in granite from Illinois borehole UPH-3 and their relationship to the rock's stress history. *Tectonophysics* **135**, 297–306.

Lespinasse, M. & Cathelineau, M. 1990. Fluid inclusions in a fault zone: a study of fluid inclusion planes in the St. Sylvestre granite, northwest Massif Central, France. *Tectonophysics* **184**, 173–187.

Neretnieks, I. 1980. Diffusion in the rock matrix: an important factor in radionuclide retardation. *J. geophys. Res.* **85**, 4379–4397.

Niemi, T. M. & Hall, T. N. 1992. Late Holocene slip and recurrence of great earthquakes on the San Andreas fault in northern California. *Geology* **20**, 195–198.

Norton, D. & Knapp, R. 1977. Transport phenomena in hydrothermal systems: the nature of porosity. *Am. J. Sci.* **277**, 913–936.

Oelkers, E. H. & Helgeson, H. C. 1988. Calculation of the thermodynamic properties of aqueous species at high pressures and temperatures: aqueous tracer diffusion coefficients of ions to 1000°C and 5 kb. *Geochim. cosmochim. Acta* **52**, 63–85.

O'Hara, K. D. 1990. Brittle-plastic deformation in mylonites: an example from the Meadow Fork thrust, western Blue Ridge province, southern Appalachians. *Bull. geol. Soc. Am.* **102**, 1700–1713.

O'Hara, K. D. 1991. Fluid inclusion evidence for basement decompression during Permo-Triassic extension, SE New England. *J. Met. Geol.* **9**, 567–579.

O'Hara, K. D. & Haak, A. 1992. A fluid inclusion study of fluid pressure and salinity variations in the footwall of the Rector Branch thrust, North Carolina. U.S.A. *J. Struct. Geol.* **14**, 579–589.

Parry, W. T. Wilson, P. N., Bruhn, R. L., 1988. Pore-fluid chemistry and chemical reactions on the Wasatch normal fault, Utah. *Geochim. cosmochim. Acta* **52**, 2053–2063.

Ramsay, J. G. 1980. The crack-seal mechanism of rock deformation. *Nature* **284**, 135–139.

Roedder, E. 1984. Fluid inclusions, volume 12 (edited by Ribbe, R. H.). *Min. Soc. Am. Reviews in mineralogy*.

Scholz, C. H., Sykes, L. R. & Argarwal, Y. P. 1973. Earthquake prediction: a physical basis. *Science* **181**, 803–810.

Scholz, C. H. 1990. *The Mechanics of Earthquakes and Faulting*. Cambridge University Press. Cambridge.

Schwartz, D. P. & Coppersmith, K. J. 1984. Fault behavior and

characteristic earthquakes: examples from the Wasatch and San Andreas fault zones. *J. geophys. Res.* **89**, 5681–5698.
Shelton, K. L. & Orville, P. M. 1980. Formation of synthetic fluid inclusions in natural quartz. *Am. Mineral.* **65**, 1233–1236.
Sibson, R. H. 1987. Earthquake rupturing as a mineralizing agent in hydrothermal systems. *Geology* **15**, 701–704.
Sibson, R. H., Moore, J. M. & Rankin, A. H. 1975. Seismic pumping—a hydrothermal fluid pumping mechanism. *J. Geol. Soc. Lond.* **131**, 653–659.
Smith, D. L. & Evans, B. 1984. Diffusional healing in quartz. *J. geophys. Res.* **89**, 4125–4133.
Sterner, S. M. & Bodnar, J. R. 1989. Synthetic fluid inclusions in quartz during re-equilibration of fluid inclusions in quartz during laboratory-simulated metamorphic burial and uplift. *J. Met. Geol.* **7**, 243–266.
Thomas, D. 1988. Geochemical precursors to seismic activity. *Pure & Appl. Geophys.* **126**, 241–267.
Tsang, C. 1991. Coupled hydromechanical–thermomechanical processes in rock fractures. *Rev. Geophys.* **29**, 537–551.
Vovk, I. F. 1987. Radiolytic salt enrichment and brines in the crystalline basement of the East European platform. In: *Saline Water and Gases in Crystalline Rocks* (edited by Fritz, P. & Frape, S. K.). *Spec. Pap. geol. Ass. Can.* **33**, 197–210.
Vrolijk, P., Fisher, A. & Gieskes, J. 1991. Geochemical and geothermal evidence for fluid migration in the Barbados accretionary prism (ODP 110). *Geophys. Res. Lett.* **18**, 947–950.

APPENDIX

The program used to calculate the diffusion profile with random recurrence intervals, is based on the flow diagram shown.

Definition of variables in flow chart

NORUPT	number of fault rupture events
C0	initial concentration for first rupture
TAU	time increment for each calculation
INTERVAL	fault recurrence interval
D	diffusion coefficient
L	diffusion distance
RND	random number (100–1000)
N	number of calculations for per event
TIME	counter for incrementing time
CEND	concentration at end of recurrence interval
TOT	total elapsed time
CE	equilibrium concentration
I	counter for number of fault rupture events
J	counter for number of concentration calculation
C(I,J)	concentration number J during rupture interval I
T(I,J)	time for concentration number J during rupture interval I.

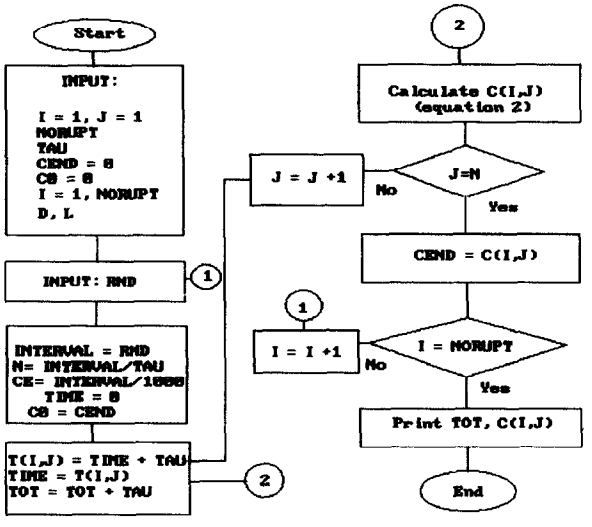

Fig. A1. Flow chart.